ELSEVIER

Earth and Planetary Science Letters 204 (2002) 307–320

EPSL

www.elsevier.com/locate/epsl

A 30 000 yr record of erosion rates from cosmogenic ^{10}Be in Middle European river terraces

M. Schaller [a,*], F. von Blanckenburg [a,1], A. Veldkamp [b], L.A. Tebbens [c], N. Hovius [d], P.W. Kubik [e]

[a] *Isotopengeologie, Universität Bern, Erlachstrasse 9a, 3012 Bern, Switzerland*
[b] *Laboratory of Soil Science and Geology, Wageningen University, P.O. Box 37, 6700 AA Wageningen, The Netherlands*
[c] *Department of Geographical Sciences, Utrecht University, P.O. Box 80.115, 3508 TC Utrecht, The Netherlands*
[d] *Department of Earth Sciences, University of Cambridge, Downing Street, Cambridge CB2 3EQ, UK*
[e] *Paul Scherrer Institut/Institute of Particle Physics, ETH Hönggerberg, CH-8093 Zürich, Switzerland*

Received 15 May 2002; received in revised form 13 August 2002; accepted 4 September 2002

Abstract

Cosmogenic ^{10}Be in river-borne quartz sand records a time-integrated erosion rate representative of an entire drainage basin. When sequestered in a terrace of known age, paleo-erosion rates may be recovered from the nuclide content of the terrace material. Paleo-erosion rates between 30 and 80 mm/kyr are determined from terrace sediments 200 to 30 000 yr in age of the Allier and Dore Rivers, France, and the Meuse (Maas) River, the Netherlands. Erosion rates determined from cosmogenic nuclides on terraces from the Allier River are consistent with rates derived from the sedimentary fill of a lake in the Allier catchment. A strong decrease in cosmogenic nuclide-derived erosion rates from terraces of the Meuse River with Late Pleistocene to Holocene age is observed. The paleo-erosion signal from cosmogenic nuclides records projection of the elevated Late Pleistocene erosion rate into the time-integrated rates derived from Middle European rivers.

Keywords: cosmogenic elements; erosion rates; terraces; climate change; Europe

1. Introduction

Important feedbacks exist between erosion and climate, tectonics, and soil production (e.g. [1–3]). Our understanding of these feedbacks depends upon the quantification of present and past erosion rates. To date, paleo-erosion rates have been determined using thermobarometry of metamorphic belts [4], fission track analysis [5], the sedi-

* Corresponding author. Present address: Department of Earth Sciences, University of Cambridge, Downing Street, Cambridge CB2 3EQ, UK. Tel.: +44-1223-333-455; Fax: +44-1223-333-450.
E-mail address: msch02@esc.cam.ac.uk (M. Schaller).

[1] Present address: Institut für Mineralogie, Universität Hannover, Callinstr. 3, 30167 Hannover, Germany.

0012-821X/02/$ – see front matter
PII: S0012-821X(02)00951-2

mentary record of natural closed basins [6], and the dissection of datable surfaces [7]. The cosmogenic nuclide inventory of river sediments has the potential to complement this array over the critical range of time scales from 10^2 yr to 10^6 yr. Cosmogenic ^{10}Be in river-borne quartz sand records a time-integrated erosion rate representative of an entire drainage basin [8–10]. When sequestered, for instance in a terrace, quartz retains part of this cosmogenic nuclide signal [11–15] until it has decayed radioactively. Thus, knowing the production and decay rates of the cosmogenic nuclide and the age of the deposit, paleo-erosion rates may be recovered from the nuclide content of terrace material. We have applied this approach to a series of Late Pleistocene and Holocene terraces of the Allier and Dore Rivers, France, and the Meuse River, the Netherlands, with the aim of quantifying the erosional response to climate change in the Late Quaternary, encompassing an age range of 30 000 to 200 yr.

2. Measuring paleo-erosion rates

The cosmogenic nuclide inventory of quartz in river sediments consists of inherited nuclides, produced before deposition, and nuclides produced by post-depositional irradiation. The former, in turn, is the figure of interest in this study, and can be attributed to irradiation prior to mobilization, or during transfer from the bedrock source to the site of deposition (cf. [11,12]). Catchment-wide paleo-erosion rates (paleo-E_C) can be calculated by removing the post-depositional component (C_{dep}) from the measured nuclide concentration (C_{total}).

Although C_{dep} is small in the Late Pleistocene and Holocene samples studied here, C_{dep} can be calculated as follows. Cosmogenic nuclides, such as ^{10}Be, are produced by spallation and by fast and stopped muons. While the mean free path for spallation production is $\sim$60 cm in silicate rocks, muons penetrate deep into the subsurface (e.g. [16]): terrace sediments are unlikely to be shielded from their impact [17]. The depth-dependence of nuclide production by post-depositional irradiation has been calculated by using the following equation fitting the nucleonic, stopped and fast muonic production (for further explanation see Appendix 1):

$$C_{dep} = \left[\left(P_{Nuc}(0)\times\sum_{i=1}^{2}a_i\times e^{\frac{-z\times\rho}{b_i}}\right) + \left(P_{\mu stopped}(0)\times\sum_{j=1}^{3}a_j\times e^{\frac{-z\times\rho}{b_j}}\right) + \left(P_{\mu fast}(0)\times\sum_{k=1}^{3}a_k\times e^{\frac{-z\times\rho}{b_k}}\right)\right]\times\frac{(1-e^{-\lambda\times t})}{\lambda} \quad (1)$$

where z (cm) is the depth below surface, t (yr) is the time since deposition, ρ (g/cm^3) is the sediment density, λ (yr^{-1}) is the decay constant for the nuclide, and $P_{Nuc}(0)$, $P_{\mu stopped}(0)$ and $P_{\mu fast}(0)$ (atoms/(g(quartz)$\times$yr)) are the local surface production rates of cosmogenic nuclides by spallation, stopped and fast muons, respectively; $a_{i,j,k}$ (dimensionless) and $b_{i,j,k}$ (g/cm^2) are coefficients for the depth scaling of the production rates (values given in Appendix 1). Nuclide production rates are also dependent on altitude and latitude: we have scaled [18–20] the post-depositional production rates for nucleons and muons to the altitude from which the sample was collected. The uncertainties for the post-depositional nuclide accumulation include errors in the determination of the burial depth and the age of the sample. The influence of secular variation of the geomagnetic field on production rates of cosmogenic nuclides is small at the latitude of the analyzed samples [21,22].

We assume that the inherited nuclide concentration C_{in} is due to irradiation of quartz during its erosion in the source area and that transport times are short in comparison. As C_{in} decreases over time due to radioactive decay, $C_{in}(t)$ at the time of sampling needs to be determined. Therefore:

$$C_{\mathrm{in}}(t) = \left[P_{\mathrm{Nuc}}(0) \times \sum_{i=1}^{2} \frac{a_i}{\left(\lambda + \frac{\rho \times E}{b_i}\right)} + P_{\mu\mathrm{stopped}}(0) \times \sum_{j=1}^{3} \frac{a_j}{\left(\lambda + \frac{\rho \times E}{b_j}\right)} + P_{\mu\mathrm{fast}}(0) \times \sum_{k=1}^{3} \frac{a_k}{\left(\lambda + \frac{\rho \times E}{b_k}\right)} \right] \times \mathrm{e}^{-\lambda \times t} \quad (2)$$

where E (cm/yr) is the erosion rate, and nuclide production rates $P_{\mathrm{Nuc}}(0)$, $P_{\mu\mathrm{stopped}}(0)$ and $P_{\mu\mathrm{fast}}(0)$ are scaled to the mean altitude and latitude of the area upstream of the sample location. For the total error in erosion rate we have considered analytical, blank, depth, and age errors. Uncertainties in scaling factors, altitude, mean altitude and the sea level production rate of neutrons can be neglected for inter-sample comparison. These uncertainties are the same for all samples and would require propagation of an additional uncertainty of up to 20% into the error of each erosion rate measurement.

Analytical techniques are described by Schaller et al. [23]. We used quartz grains of 0.5–1 mm in size. Cosmogenic nuclide-derived erosion estimates are assumed to be independent of grain size. This is justified by the conclusion of Schaller et al. [23] that there is no grain size control on erosion rates calculated from the bedload of modern Middle European rivers.

Schaller et al. [23] have summarized the potential biases introduced into erosion rate estimates, due for instance to sudden regolith mixing [10], selective dissolution of other minerals than quartz [24], or deposition of loess or volcanic ash during erosion. In terrace studies, additional uncertainties may arise from partial erosion of the terrace overburden and exhumation of quartz sand to the surface. Partial erosion would lead to an overestimate of the production rate. For example, calculated paleo-erosion rates could be overestimated by up to 8% in the case of 1 m of recent lowering of the terrace top for a terrace 2 kyr in age. This effect diminishes rapidly with increasing burial depth and is largely avoided by sampling more than 1 m below the terrace surface. Water in any form shields against cosmic ray impact. Thus, in a (partially) glaciated catchment, cosmogenic nuclide concentrations in the substrate remain low compared to the unglaciated equivalent. Calculated paleo-E_C for glaciated catchments are, therefore, too high (for further discussion see Appendix 2).

The quartz content of the lithologies is assumed to be uniform throughout the catchments. Production rates for erosion rate calculation have been determined from the mean altitude of each sample's upstream catchment area and are regarded as uniform. This simplification introduces negligible uncertainties (for further discussion see Appendix 1). Furthermore, today's upstream topography is very similar for all samples from a given terrace sequence. Therefore, the uncertainty in production rates arising from the use of mean altitude is unimportant for inter-sample comparison.

3. Sampling sites

In order to determine the feasibility of cosmogenic nuclide-derived paleo-erosion rates (paleo-E_C) from the cosmogenic nuclide inventory of sequestered sediments, we selected a sampling site with the following attributes: (1) the presence of a sequence of quartz-bearing deposits covering a range of known ages; and (2) the availability of an independent record of paleo-erosion rates for the same area and time interval. These requirements are met at the confluence of the Allier and Dore Rivers in the Massif Central, France. There, a flight of at least eight river terraces [25] has formed in the Oligocene Limagne rift (Fig. 1A). Whereas the highest parts of the Allier basin, including the isolated Cantal and Mont Dore volcanoes and Montagne de la Margeride were glaciated during the Last Glacial Maximum (LGM), the Dore basin has remained largely free of ice

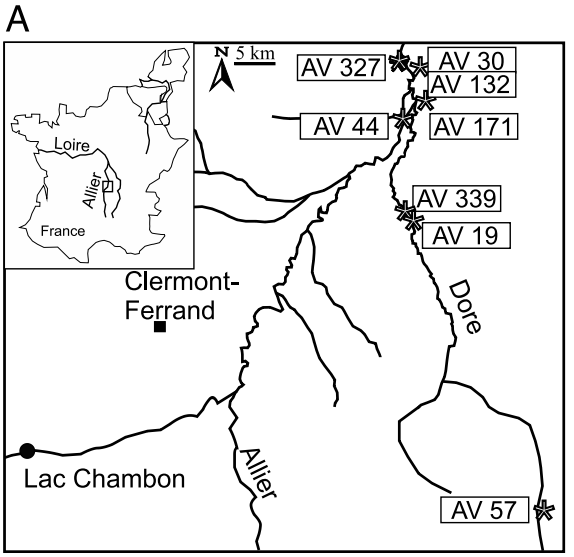

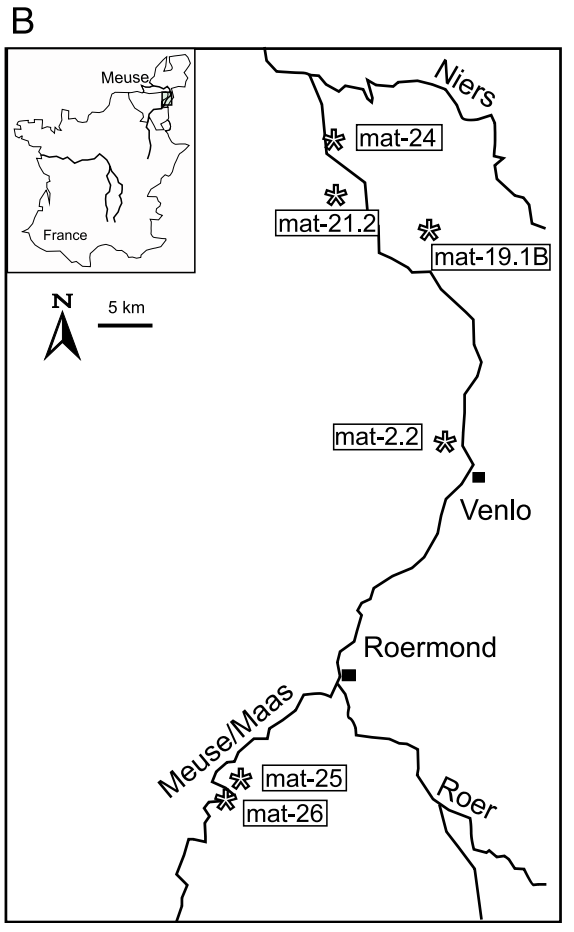

[26]. The eight main terrace levels at the Allier–Dore confluence are labelled z (present river bed) to s (oldest terrace level) (Table 1). The lowermost three main terrace levels (x to z), which are used in this study, have been dated to LGM to Holocene by ^{14}C [27].

A second sampling site is the terrace sequence of the Meuse River, the Netherlands (Fig. 1B). Near Roermond, an extensive flight of river terraces dating back to 4 Myr dominates the lower Meuse valley [28]. The LGM to Holocene terraces have been sampled for this study (Table 2). Upstream of our sample locations the Meuse basin has not been glaciated in the Late Pleistocene.

4. Results and discussion

4.1. Application to the Allier terrace sequence

Paleo-E_C determined in the terraces along the Allier River vary between 40 and 70 mm/kyr (Fig. 2; Table 3). The lowest value is for the oldest terrace sample, whereas the highest value is for the terrace deposited at the Pleistocene to Holocene transition. Paleo-E_C determined from cosmogenic nuclides in quartz from Dore terraces are 48–53 mm/kyr and remained constant within error between ~15 kyr and ~5 kyr (Fig. 2). Thus the Allier and Dore catchments appear to have different erosion histories. This may have been caused by differences in glaciation history and relief between the catchments. In contrast to the Dore catchment, the highest 25% of the Allier catchment was partially covered by ice during the LGM [26]. This glaciation may have given rise to elevated erosion rates as many glaciers erode faster than the rivers they have replaced [29]. In addition glaciation may also have reduced cosmogenic irradiation of the rock mass. Complete shielding of the highest 25% of the Allier

←

Fig. 1. (A) Map of the Allier catchment showing location of terrace samples (stars) analyzed for cosmogenic ^{10}Be, and Lac Chambon where the lake fill record was used to estimate paleo-erosion rates [6]. (B) Map of the Meuse catchment showing locations of terrace samples.

Table 1
Terrace stratigraphy in the Allier and Dore basin

Terrace stratigraphy[a]	Sublevels	Deposition age[b] (yr BP)	Dating method	Analyzed samples	
				Allier	Dore
Fs					
Ft					
Fu	Fua				
	Fub				
Fv	Fva_I	~600 000	Ar/Ar		
	Fva_{II}				
	Fvb				
Fw	Fwa				
	Fwb_I	120 000–160 000 (±10 000)	U–Th		
	Fwb_{II}	120 000 (±13 000)	U–Th		
Fx	Fx_I	29 560 (±330)	^{14}C	AV 132	
	Fx_{II}	16 558 (±250)–29 560 (±330)	^{14}C	AV 327	
	Fx_{III}	12 370 (±230)–16 558 (±250)	^{14}C	AV 171	AV 19
	Fx_{IV}	9 630 (±90)–11 380 (±100)	^{14}C	AV 30	AV 57
Fy		7 310 (±70)–9 630 (±90)	^{14}C		
Fz		<5 000	^{14}C	AV 44	AV 339

[a] Terrace stratigraphy as given in Larue [39] and Pastre [40].
[b] Ages as given in Veldkamp and Kroonenberg [27].

catchment from 30 kyr to 20 kyr would have resulted in an increase of up to 35% of apparent late glacial erosion rates as calculated from cosmogenic nuclides (glaciation-corrected values in Fig. 2, for further explanation see Appendix 2).

Alternatively, Schaller et al. [23] have found that ΔH_{mean} (mean elevation minus minimum elevation of the basin) correlates well with erosion rates in Middle European catchments. ΔH_{mean} is significantly lower in the Dore catchment (400 m) than in the Allier basin (700 m). The elevated paleo-E_C in the Allier basin may arise in part from the greater local relief.

Paleo-E_C may be tested against other erosion data for the Allier region (Fig. 2). River load measurements have been used to calculate physical and chemical erosion rates at various stations within the study area [23]. These conventional, present-day erosion rates vary between 3 and 8 mm/kyr, and are up to 10 times lower than paleo-E_C.

The nuclide approach has been applied to quartz sand from the active channel of the Allier River in the vicinity of the terrace localities. Cosmogenic nuclide-derived erosion rates (E_C) from modern bedload range from 40 mm/kyr to 73 mm/kyr (recalculated values from [23] as given in Appendix 1) and overlap largely with paleo-

Table 2
Terrace stratigraphy in the Meuse basin

Terrace stratigraphy	Deposition age[a] (yr BP)	Dating method	Analyzed samples
Weichselian[a]	13 280 (±70)–22 000	^{14}C	mat-2.2
	13 280 (±70)–12 110 (±70)	^{14}C	mat-19.1B
	11 280 (±80)	^{14}C	mat-21.2
Holocene[b]	3 124 (±60)	^{14}C	mat-24
	1 350–1 650	^{14}C	mat-25.2
	<200	^{14}C	mat-26

[a] Ages as given in Tebbens et al. [41].
[b] Ages as given by the Geological Survey of The Netherlands except sample mat-24 which has been dated for this study.

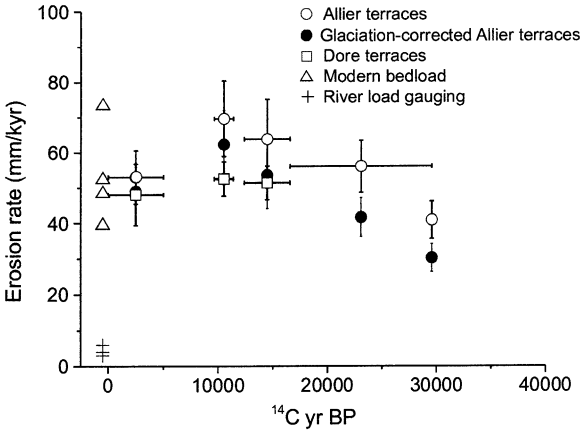

Fig. 2. Erosion rates calculated from cosmogenic ^{10}Be concentrations in Allier and Dore terraces of known age and in modern Allier and Dore bedload samples, and from river load gauging. Filled circles represent cosmogenic nuclide-derived erosion rates using production rates corrected for shielding due to glaciation of the Allier basin from 30 kyr to 20 kyr.

E_C. Notably, this range is larger than the range of paleo-E_C obtained from terrace samples. We do not believe that this difference is related to the limited number of terrace samples used in this study. Instead, we speculate that it may reflect the processes of sediment production. Under periglacial conditions, hillslopes are less prone to linear dissection than during warmer, wetter times. Uniform lowering of the landscape during periglacial times would give rise to sediment with a relatively homogeneous cosmogenic nuclide concentration. In contrast, present-day bedload and Holocene sediments have been liberated, in part, by rill and gully erosion. These processes sample the soil and regolith profile over a greater depth and therefore generate sediment with a more diverse cosmogenic nuclide concentration. In addition, anthropogenic activity may have contributed to the enhanced heterogeneity of E_C from present-day bedload samples. The singularly high erosion rate of 73 mm/kyr reported for a bedload sample from the Allier is probably the result of changed land use (recalculated for sample loi-19, [23], Appendix 1).

Neither river load measurements nor E_C from bedload cover the temporal range of our terrace study. The best opportunity to validate the paleo-E_C is offered by the sedimentary record contained in Lac Chambon, situated in the upper Allier catchment (Fig. 1). Macaire et al. [6] have calculated mechanical erosion rates in the Allier headwaters from the sediment accumulation history of this closed basin. Their record (Fig. 3) starts at 12 600 ^{14}C yr BP (Bølling/Allerød) with erosion rates of 49 ± 15 mm/kyr. The highest erosion rates are reported for the Subatlantic (166 ± 50 mm/kyr) and the Younger Dryas (120 ± 36 mm/kyr). The paleo-erosion rates calculated from the Lac Chambon fill are higher than paleo-E_C from cosmogenic nuclides in Allier and Dore terraces. This may be due to differences in catchment size, topography and lithology. With a catchment area of 40 km^2 Lac Chambon is two orders of magnitude smaller than the Allier and Dore basin. Lac Chambon is located near the highest point of the Allier basin (Puy de Sancy, 1885 m a.s.l.) and its catchment comprises some of the steepest relief in the region. The occurrence of large landslides near the lake [30] indicates that this relief is subject to active erosion. 70% of the area feeding Lac Chambon is underlain by mafic volcanic rocks [6], whereas the Allier and Dore catchments are dominated by more resistant, crystalline basement rocks. Finally, paleo-E_C are strongly dampened by the considerable lag-time required for the cosmogenic nuclide budget to settle back into a new steady state after a change in erosion rate [8]. Because of this lag-time, E_C depend strongly on the erosion history.

The abundance of cosmogenic nuclides in well-

Table 3
Cosmogenic nuclide-derived erosion rate data

Drainage basin	Sample	Altitude	Latitude		Upstream catchment mean[a]		Sampling depth	Deposition age[b]	Error[c]	Total ^{10}Be concentration[d]	Pre-depositional ^{10}Be concentration[e]	Erosion rate[f]	Error[g]	Pre-depositional apparent age[h]
		(m)	N	E	altitude (m)	latitude N	(m)	(^{14}C yr BP)	(^{14}C yr)	(10^5 atoms/g(quartz))	(10^5 atoms/g(quartz))	(mm/kyr)	(mm/kyr)	(kyr)
Allier	AV 132	271	46°03′	3°27′	790	45°	7.00 ± 0.50	29 560	330	1.97 ± 0.23	1.97 ± 0.23	40.8	5.3	19.3
	AV 327	275	46°03′	3°28′	790	45°	2.00 ± 0.20	16 600–29 600	6 500	1.52 ± 0.18	1.45 ± 0.18	56.0	7.4	14.2
	AV 171	283	46°01′	3°29′	790	45°	2.80 ± 0.20	12 400–16 600	3 000	1.30 ± 0.22	1.28 ± 0.22	63.8	11.3	12.5
	AV 30	271	46°03′	3°27′	790	45°	2.20 ± 0.20	9 600–11 400	900	1.20 ± 0.17	1.17 ± 0.17	69.6	10.8	11.5
	AV 44	263	46°00′	3°27′	860	45°	0.05 ± 0.01	< 5 000	2 500	1.77 ± 0.16	1.61 ± 0.23	53.0	7.6	14.9
Dore	AV 19	299	45°54′	3°28′	730	45°	2.00 ± 0.10	12 400–16 600	2 100	1.56 ± 0.11	1.52 ± 0.11	51.4	4.8	15.6
	AV 57	535	45°31′	4°00′	850	45°	1.00 ± 0.10	9 600–11 400	900	1.80 ± 0.12	1.62 ± 0.12	52.5	4.8	15.0
	AV 339	281	45°55′	3°27′	730	45°	0.05 ± 0.01	< 5 000	2 500	1.78 ± 0.25	1.62 ± 0.30	48.0	8.7	16.6
Meuse	mat-2.2	24	51°24′	6°08′	268	51°	2.20 ± 0.20	13 300–22 000	4 400	0.77 ± 0.11	0.73 ± 0.11	81.1	12.7	10.7
	mat-19.1B	20	51°34′	6°06′	263	51°	4.00 ± 0.40	12 100–13 300	600	0.88 ± 0.09	0.88 ± 0.09	67.0	7.6	12.9
	mat-21.2	15	51°37′	5°59′	263	51°	2.30 ± 0.20	11 280	80	1.00 ± 0.09	0.98 ± 0.09	59.9	6.2	14.4
	mat-24	11	51°40′	5°59′	263	51°	5.00 ± 1.00	3 124	60	1.07 ± 0.16	1.07 ± 0.16	54.6	8.9	15.7
	mat-25.2	26	51°07′	5°51′	282	50°	0.40 ± 0.10	1 350–1 650	150	1.85 ± 0.13	1.85 ± 0.13	30.9	2.7	27.0
	mat-26	25	51°06′	5°19′	282	50°	0.10 ± 0.03	< 200	100	1.87 ± 0.15	1.81 ± 0.15	30.5	2.8	27.3

[a] Mean altitude and latitude to determine production rate for paleo-erosion rate calculation.
[b] Allier/Dore: Ages given in Veldkamp and Kroonenberg [27]; the ages used for calculation are the mean of the ^{14}C dated terraces. For samples AV 44 and AV 339 an age of 2500 yr is assumed for the calculation. Meuse: Ages given by the Geological Survey of The Netherlands and Tebbens et al. [41] except sample mat-24 which has been dated for this study; the ages used for calculation are the mean of the ^{14}C dated terraces. For sample mat-26 an age of 100 yr is assumed for the calculation.
[c] Allier/Dore: Error is the deviation of the minimum and maximum age from the mean age. For sample AV 132 the error is the error resulting from ^{14}C dating as given in Veldkamp and Kroonenberg [25]. Meuse: Error is the deviation of the minimum and maximum age from the mean age. For samples mat-21.2 and mat-24 the errors are the errors resulting from ^{14}C dating.
[d] ^{10}Be concentration with analytical error (1σ).
[e] Pre-depositional ^{10}Be concentration with combined analytical (1σ), age and depth error.
[f] Paleo-erosion rates calculated from pre-depositional nuclide concentration using Eq. 2 which is based on the formalism developed by Lal [38].
[g] For inter-sample comparison: Combined analytical, blank, depth, and age error.
[h] Corresponding to the mean period spent in the uppermost ~60 cm of the eroding substrate.

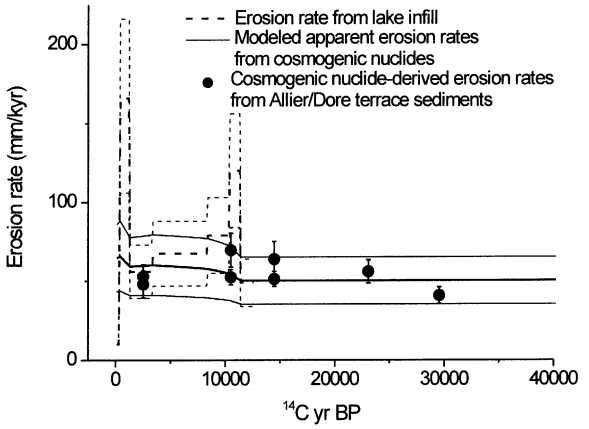

Fig. 3. Erosion rates calculated from sedimentary fill of Lac Chambon back to 12 600 ^{14}C yr (after [6]). Error margins are shown as thin dotted lines. Solid line shows the cosmogenic nuclide-derived erosion record predicted from a numerical model of the Lac Chambon erosion history and assuming a constant erosion rate prior to 12 600 yr. Associated error margins are shown as thin lines. Cosmogenic nuclide-derived erosion rates measured in Allier terraces are included for comparison.

mixed sediments can be predicted by numerical integration of the depth-dependent production rate of nucleons and fast and stopped muons in a vertical source material section experiencing variable model erosion rates [8]. We used this method to convert the Lac Chambon erosion record into paleo-E_C, assuming that no regolith mixing did occur during sediment production (cf. [10,31]). Taking into account complete mixing of regolith would add a further time lag to actual erosion rates. The deeper the regolith is mixed, the greater the time required for the cosmogenic nuclide signal to match actual erosion rates. For the period before 12 600 ^{14}C yr BP, the cosmogenic nuclide abundance was run to steady state using an erosion rate as reported from the Bølling/Allerød. After that, input erosion rates were varied between 49 and 166 mm/kyr in a sequence closely following the lacustrine record of erosion in the upper Allier catchment (Fig. 3). Notably, paleo-E_C predicted for this sequence range between 50 and 70 mm/kyr. Predicted rates fit well the paleo-E_C measured in the Allier terraces. However, the erosion rate before the Bølling/Allerød is not known from the lake record and alternative erosion scenarios are possible. For example, erosion rates may have been highest during the LGM and lower in pre- and post-LGM time. This would suppress the predicted peak values of paleo-E_C for the Lac Chambon record. In fact, our terrace data set is compatible with various scenarios of fluctuating Late Pleistocene erosion rates that have been dampened by the time lag inherent in the cosmogenic method. However, the data can also roughly be fitted with a constant erosion rate model of 50 mm/kyr throughout. More conclusive evidence of erosion rate changes comes from the nearby Meuse River which cuts through the Ardennes Mountains of Belgium on its way to the North Sea.

4.2. Application to the Meuse terrace sequence

Paleo-E_C determined in the Meuse terraces decrease steadily from 81 mm/kyr in the Late Pleistocene to 31 mm/kyr in the Holocene (Fig. 4, Table 3). Late Holocene values agree well with E_C calculated for bedload samples taken from the active river channel in the terrace area. Using the numerical integration approach discussed in the previous section, the time series of cosmogenic rates can be modeled by a change of erosion rate

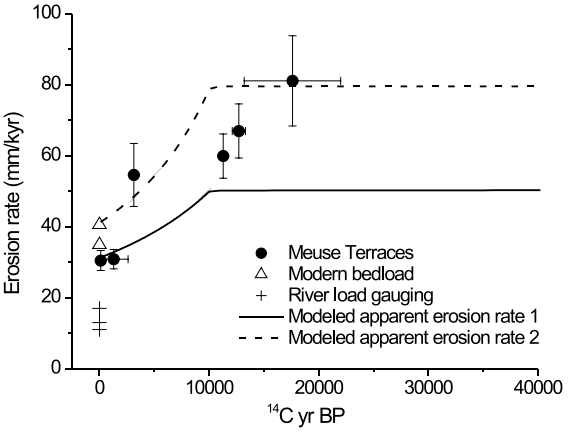

Fig. 4. Erosion rates calculated from cosmogenic ^{10}Be concentrations in Late Pleistocene to Holocene Meuse terraces of known ages and in modern river sediment, and from river load gauging. Input erosion rates of 50 mm/kyr and 80 mm/kyr during the Pleistocene and zero erosion during the Holocene time are used to model cosmogenic nuclide-derived apparent erosion rates.

from Late Pleistocene to Holocene (Fig. 4). A constant erosion rate model is not compatible with this data set, even when expanding analytical errors to the 2σ level. We conclude that in the Meuse catchment LGM erosion rates were higher than Holocene rates.

4.3. Modern river loads

These results shed light on an important observation made in earlier cosmogenic nuclide studies of Middle European rivers. E_C for bedload samples from the active channels of these rivers are 1.5–10 times higher than estimates based upon 100 yr gauging records of their suspended and dissolved loads ([23]; after recalculation as given in Appendix 1). A similar observation was made in the Idaho mountains of the temperate US [32]. Kirchner et al. [32] and Schaller et al. [23] have suggested that this discrepancy might be due to systematic underestimation of modern river loads. Schaller et al. [23] have offered two further explanations: (a) spatially non-uniform erosion (e.g. linear dissection) and selective tapping of deeper segments of the irradiation profile; and (b) inheritance of a Late Pleistocene erosion signal. Explanation (a) can not be entirely excluded as linear landscape dissection during the Holocene may have caused part of the scatter in E_C observed in modern river bedload. However, continuity requires that the absence of linear dissection in the Late Pleistocene followed by increased linear dissection during the Holocene would not only have resulted in higher apparent E_C in modern bedload, but also in lower rates in pre-Holocene erosion products. This is not observed. Therefore, inheritance of a Late Pleistocene erosion signal remains as a likely explanation.

5. Conclusions

Cosmogenic nuclide studies of fluvial deposits offer new and robust constraints on paleo-erosion rates. Cosmogenic nuclide-derived paleo-erosion rates from terraces flanking the Allier and Dore Rivers in France agree well with independent estimates from Lac Chambon, located within the upper Allier catchment. This validates our method, and allows us to apply it in nearby, similar catchments.

Paleo-erosion estimates for the Meuse catchment, located at a slightly higher latitude, indicate that erosion rates have been enhanced during the Last Glacial Maximum, when periglacial processes prevailed throughout the catchment. The climate-driven changes in real erosion rates are dampened in the cosmogenic nuclide record of river sediments because the method integrates over long time intervals. As a result the Late Pleistocene signal is propagated into the cosmogenic nuclide-derived erosion estimates for the present-day bedload of Middle European rivers.

Acknowledgements

We gratefully acknowledge laboratory assistance by I. Hebeisen and A. Brockmann and thank M.W. van den Berg for stimulating discussion. Comments by P. Bierman, D.E. Granger and J.W. Kirchner helped to improve an earlier version of the manuscript. This study was supported by the Schweizerische Nationalfond (Grant 2100-053971 to F.v.B.).*[BARD]*

Appendix 1. A re-evaluation of cosmogenic nuclide production rates and revision of Schaller et al. [23] erosion rates

Heisinger et al. [19,20] have recently re-evaluated their original sea level high latitude (SLHL) production rates and their depth-dependence [33,34]. This re-evaluation necessitates a recalculation of the nucleonic SLHL production rate as presented by Schaller et al. [23], which was based on the ^{10}Be SLHL production rate at Köfels (1.68 km altitude, 47° latitude) of Kubik et al. [35].

The new values for the stopped muonic (0.106 atoms/(g(quartz)×yr)) and fast muonic (0.093 atoms/(g(quartz)×yr)) ^{10}Be production rates at SLHL were scaled to the Köfels altitude with an absorption mean free path of 247 g/cm^2 [36] for

stopped muons and the formalism suggested in Heisinger et al. [19,20] for fast muons. According to Allkofer [37], the latitude effect in the muonic component becomes negligible above 40° latitude. The locally produced muon concentration was subtracted from the measured concentrations at the Köfels site to obtain the local nucleonic production rate. This nucleonic component was then scaled down to SLHL using the scaling of Dunai [18] resulting in a spallation production rate of 5.33 ± 0.34 atoms/(g(quartz)×yr). For all our calculations we have now used the Dunai [18] formalism rather than that of Lal [38]. The Dunai formalism allows for separate atmospheric scaling of nucleonic, stopped muonic, and fast muonic production, respectively. The scaling formalism of the latter has now become available [19,20]. However, using the scaling formalism for nucleons of Dunai results in only 5–7% lower nucleonic production than proposed by Lal [38].

Using an exponential depth-dependence for the production rates below a surface allows the expression of a calculated nuclide concentration as a function of time and erosion rate in an explicit form [38]. In order to maintain this formalism, the depth-dependences of stopped and fast muons calculated by Heisinger et al. ([19,20]; eqs. 11 and 14, respectively) were approximated by a fit with three exponential functions (Table A1.1) allowing sufficiently accurate description of the muonic nuclide production down to more than 20 m depth. The difference between this fit and the Heisinger et al. calculations is less than 1% for stopped as well as fast muons at 20 m depth. A very good description of muonic nuclide production down to 300 m depth can be obtained with five exponential functions. For fast erosion (>100 mm/kyr), erosion rates calculated with three exponential functions differ only 2% from erosion rates calculated with the five exponential functions. For lower erosion rates the difference is even smaller, because the fraction of muon-produced nuclides has been reduced by radioactive decay. The fit with three exponential functions can be used to calculate the post-depositional production in river terrace studies. During the re-evaluation of the muonic depth-dependence of production rates, an error in nucleonic depth-dependence calculation ([23], Table 3) has been discovered and corrected. All new parameters are given in Table A1.1.

These revisions in production rates and depth-dependence parameters make a re-evaluation of the erosion rates from Schaller et al. [23] necessary. To allow for comparison with the new terrace results presented here, erosion rates from modern river bedload ([23], Table 2) have been recalculated with the above described changes (Table A1.2). All these corrections lead to erosion rates which are 27–33% higher than erosion rates published by Schaller et al. [23]. The main cause of this increase is the higher production rate for fast muons, and their low absorption coefficients at depth [19].

Schaller et al. [23] have determined the production rate from the mean altitude instead of averaging the production rates derived from all altitudes in the catchment. This simplification is justified as the uncertainties introduced are typically only 1–2%. Even in the catchments with the

Table A1.1
Coefficients for the development of the depth-dependency

Index	Production mechanism	a	b (g/cm^2)
$i=1$	nucleonic	1.0747	157
$i=2$	$P_{Nuc}=5.33$ atoms/(g(quartz)×yr)	−0.0747	5.887
$j=1$	stopped muonic	−0.050	160
$j=2$	$P_{\mu stopped}=0.106$ atoms/(g(quartz)×yr)	0.845	1 030
$j=3$		0.205	3 000
$k=1$	fast muonic	0.010	100
$k=2$	$P_{\mu fast}=0.093$ atoms/(g(quartz)×yr)	0.615	1 520
$k=3$		0.375	7 600

Table A1.2
Recalculated catchment-wide erosion rates of Schaller et al. [21]

Sample[a]	Erosion rate (mm/kyr)	Error[b] (mm/kyr)	Total error[c] (mm/kyr)	Apparent age (yr)
reg-5	30.7	4.8	5.3	25.9
reg-7	29.6	2.8	3.0	26.7
reg-11	24.8	2.4	2.5	31.9
reg-12A	31.7	3.6	3.7	24.7
reg-12	31.6	2.9	2.9	24.8
reg-12D	30.4	5.8	6.5	25.7
reg-13	33.1	3.1	3.2	23.6
reg-14	26.6	2.5	2.6	29.1
reg-18A	32.9	6.7	8.1	23.2
reg-18	33.8	3.4	3.5	22.6
reg-18C	37.7	4.4	4.6	20.4
reg-19	30.4	3.0	3.2	25.1
reg-19	30.4	3.0	3.1	25.1
reg-20	35.2	3.3	3.4	21.9
neck-1	59.2	6.4	6.5	13.5
neck-2	109.8	15.4	16.2	7.4
neck-3	116.1	17.6	18.8	7.2
neck-4	103.8	12.0	11.8	8.0
neck-5	103.3	12.1	12.0	8.2
neck-6	89.1	9.2	9.4	9.5
neck-6	113.3	13.6	14.1	7.5
neck-6D	75.1	11.0	12.0	11.2
neck-7	121.9	16.3	17.2	7.0
neck-7	130.5	20.0	21.7	6.5
neck-8	143.6	17.0	18.0	5.9
neck-10	55.2	7.7	8.5	14.5
meu-1	28.4	2.5	2.5	28.9
meu-4	18.6	1.9	2.1	43.2
meu-7	22.5	2.5	2.7	36.3
meu-9	37.7	3.8	3.9	22.3
meu-10	29.0	4.8	5.3	28.6
meu-13A	23.9	3.7	4.3	34.3
meu-13	34.9	4.6	5.0	24.0
meu-13D	75.5	11.6	12.7	11.5
meu-14	40.6	3.8	3.9	20.9
meu-15C	80.0	9.2	9.6	10.9
meu-15C	60.2	6.4	6.6	14.3
loi-2	47.0	5.9	6.2	17.6
loi-2	47.0	6.5	7.0	17.6
loi-7	38.3	4.5	4.7	21.3
loi-10	39.5	5.2	5.5	20.5
loi-11	36.8	6.1	7.1	22.2
loi-12	47.4	6.4	7.0	17.0
loi-12	51.2	6.7	7.3	15.8
loi-14A	53.1	6.8	7.4	15.1
loi-14	47.0	6.7	7.3	17.0
loi-15	58.7	7.5	8.0	13.7
loi-17	52.4	5.0	5.2	15.2
loi-18	48.5	5.0	5.2	16.5
loi-19	73.4	9.4	9.9	10.8
loi-21	39.5	5.4	5.8	19.7
loi-23	58.9	6.2	6.4	13.3
loi-25A	57.0	7.5	8.0	13.4

Table A1.2 (*Continued*).

Sample[a]	Erosion rate (mm/kyr)	Error[b] (mm/kyr)	Total error[c] (mm/kyr)	Apparent age (yr)
loi-25	61.5	7.6	8.0	12.5
loi-29	54.7	7.1	7.6	14.3
loi-32	38.3	4.3	4.6	20.1
loi-33	41.3	5.0	5.4	18.3
loi-34	30.8	3.2	3.3	24.3
loi-36	42.1	5.3	5.7	17.9
loi-37	89.6	12.7	13.6	8.6
loi-39	78.1	10.0	10.6	10.2
loi-40	59.6	7.7	8.3	13.4
loi-41	32.5	3.7	4.1	24.6
loi-45	25.6	2.5	2.7	33.3
loi-48	7.1	0.5	0.6	104.9
loi-49	14.0	1.1	1.2	56.6
loi-50	23.0	1.8	1.9	35.8
loi-51	13.4	1.2	1.3	59.4
loi-52	30.0	2.6	2.7	27.0
loi-54	21.5	2.0	2.1	37.4
loi-55	38.0	3.9	4.0	21.1
loi-56	24.4	2.5	2.6	33.3

[a] A = grain size 1–2 mm, C = grain size 0.25–0.5 mm, D = grain size 0.125–0.25 mm, no letter grain size 0.5–1 mm.
[b] For inter-sample comparison: combined analytical, altitude (5%) and scaling factor error.
[c] For inter-method comparison: combined analytical, altitude (5%), scaling factor and production rate error.

highest relief investigated by Schaller et al. [23] the bias introduced was less than 5%. This is negligible when compared to all other uncertainties.

Appendix 2. Correction for shielding by glaciation

Glaciers shield bedrock and regolith from irradiation by cosmic rays. The production rate of nuclides in the partially shielded rock is reduced. If this additional shielding is not taken into account, an erosion rate, calculated in the way described in this paper, is an overestimate of true erosion rate. The more time has passed since the end of glaciation, the smaller this bias will be, since the 'glacial memory' is continuously being erased by erosion.

Therefore, for a correction procedure appropriate to the studied setting, the following assumptions were made. First, the uppermost 25% of the catchment has been glaciated. Second, the interval of glaciation was 30–20 kyr. Third, during the onset of glaciation the entire soil cover was removed to expose bedrock, and the cosmogenic nuclide concentration was reduced to zero. Fourth, over the period of glaciation the bedrock has been completely shielded. Fifth, following glaciation the bedrock was eroded at a constant rate with the cosmogenic nuclide-derived erosion rate that was determined prior to the correction for that sample. Sixth, the eroded material was either exported from the catchment or stored in a terrace, and no remobilization of sediment occurred. From these assumptions the reduction in production due to glaciation can be inferred. The 'reduced' apparent production rate allows recalculation of a corrected erosion rate. Corrections obtained by this method result in erosion rates which are 26% lower than original estimates.

References

[1] M.E. Raymo, W.F. Ruddiman, Tectonic forcing of Late Cenozoic climate, Nature 359 (1992) 117–122.
[2] A.M. Heimsath, W.E. Dietrich, K. Nishiizumi, R.C. Finkel, The soil production function and landscape equilibrium, Nature 388 (1997) 358–361.
[3] S.D. Willett, Orogeny and orography, the effects of ero-

sion on the structure of mountain belts, J. Geophys. Res. B Solid Earth Planets 104 (1999) 28957–58982.
[4] A.R. Philpotts, Principles of Igneous and Metamorphic Petrology, Prentice-Hall, Englewood Cliffs, NJ, 1990, 498 pp.
[5] A.J.W. Gleadow, R.W. Brown, Fission-track thermochronology and the long-term denudational response to tectonics, in: M.A. Summerfield (Ed.), Geomorphology and Global Tectonics, Wiley, New York, 2000, pp. 57–75.
[6] J.-J. Macaire, G. Bossuet, A. Choquier, C. Cocirta, P. De Luca, A. Dupis, I. Gay, E. Mathey, P. Guenet, Sediment yield during Late Glacial and Holocene periods in the Lac Chambon watershed, Massif Central, France, Earth Surf. Process. Landf. 22 (1997) 473–489.
[7] L.D. Abbott, E.A. Silver, R.S. Anderson, R. Smith, J.C. Ingle, K.A. King, D.W. Haig, E.E. Small, J. Galewsky, W.V. Sliter, Measurement of tectonic surface uplift in a young collisional mountain belt, Nature 385 (1997) 501–507.
[8] P. Bierman, E.J. Steig, Estimating rates of denudation using cosmogenic isotope abundances in sediment, Earth Surf. Process. Landf. 21 (1996) 125–139.
[9] E.T. Brown, R.F. Stallard, M.C. Larsen, G.M. Raisbeck, F. Yiou, Denudation rates determined from the accumulation of in situ-produced ^{10}Be in the Luquillo Experimental Forest, Puerto Rico, Earth Planet. Sci. Lett. 129 (1995) 193–202.
[10] D.E. Granger, J.W. Kirchner, R. Finkel, Spatially averaged long-term erosion rates measured from in situ-produced cosmogenic nuclides in alluvial sediment, J. Geol. 104 (1996) 249–257.
[11] R.S. Anderson, J.L. Repka, G.S. Dick, Explicit treatment of inheritance in dating depositional surfaces using in situ ^{10}Be and ^{26}Al, Geology 24 (1996) 47–51.
[12] G.S. Hancock, R.S. Anderson, O.A. Chadwick, R.C. Finkel, Dating fluvial terraces with ^{10}Be and ^{26}Al profiles: application to the Wind River, Wyoming, Geomorphology 27 (1999) 41–60.
[13] D.E. Granger, A.L. Smith, Dating buried sediments using radioactive decay and muogenic production of ^{26}Al and ^{10}Be, Nucl. Instrum. Methods Phys. Res. B 172 (2000) 822–826.
[14] D.E. Granger, P.F. Muzikar, Dating sediment burial with in situ-produced cosmogenic nuclides: theory, techniques, and limitations, Earth Planet. Sci. Lett. 188 (2001) 269–281.
[15] D.E. Granger, D. Fabel, A.N. Palmer, Plio-Pleistocene incision of the Green River, Kentucky, from radioactive decay of cosmogenic ^{26}Al and ^{10}Be in Mammoth Cave sediments, Geol. Soc. Am. Bull. 113 (2001) 825–836.
[16] E.T. Brown, D.L. Bourlès, F. Colin, G.M. Raisbeck, F. Yiou, S. Desgarceaux, Evidence for muon-induced production of ^{10}Be in near-surface rocks from the Congo, Geophys. Res. Lett. 22 (1995) 703–706.
[17] D.E. Granger, J.W. Kirchner, R.C. Finkel, Quaternary downcutting rate of the New River, Virginia, measured from different decay of cosmogenic ^{26}Al and ^{10}Be in cave-deposited alluvium, Geology 25 (1997) 107–110.
[18] T.J. Dunai, Scaling factors for production rates of in situ produced cosmogenic nuclides: a critical reevaluation, Earth Planet. Sci. Lett. 176 (2000) 157–169.
[19] B. Heisinger, D. Lal, A.J.T. Jull, P.W. Kubik, S. Ivy-Ochs, S. Neumaier, K. Knie, V. Lazarev, E. Nolte, Production of selected cosmogenic radionuclides by muons: 1. Fast muons, Earth Planet. Sci. Lett. 200 (2002) 345–355.
[20] B. Heisinger, D. Lal, A.J.T. Jull, P.W. Kubik, S. Ivy-Ochs, K. Knie, E. Nolte, Production of selected cosmogenic radionuclides by muons: 2. Capture of negative muons, Earth Planet. Sci. Lett. 200 (2002) 357–369.
[21] J. Masarik, M. Frank, J.M. Schäfer, R. Wieler, Correction of in situ cosmogenic nuclide production rates for geomagnetic field intensity variations during the past 800,000 years, Geochim. Cosmochim. Acta 65 (2001) 2995–3003.
[22] T.J. Dunai, Influence of secular variation of the geomagnetic field on production rates of in situ produced cosmogenic nuclides, Earth Planet. Sci. Lett. 193 (2001) 197–212.
[23] M. Schaller, F. von Blanckenburg, N. Hovius, P.W. Kubik, Large-scale erosion rates from in situ-produced cosmogenic nuclides in European river sediments, Earth Planet. Sci. Lett. 188 (2001) 441–458.
[24] E.E. Small, R.S. Anderson, G.S. Hancock, Estimates of the rate of regolith production using ^{10}Be and ^{26}Al from an alpine hillslope, Geomorphology 27 (1999) 131–150.
[25] A. Veldkamp, S.B. Kroonenberg, The application of bulk sand geochemistry in Quaternary research. A methodological study of the Allier and Dore terrace sands (Limagne, France), Appl. Geochem. 8 (1993) 177–187.
[26] Y. Veyret, Quelques caractères d'une moyenne montagne englacée, exemple des hautes terres cristallines et volcaniques du massif central francaise, Rev. Géomorphol. dynam. 29 (1980) 49–65.
[27] A. Veldkamp, S.B. Kroonenberg, Late Quaternary chronology of the Allier terrace sediments (Massif Central, France), Geol. Mijnb. 72 (1993) 179–192.
[28] M.W. van den Berg, T. van Hoof, The Maas terrace sequence at Maastricht, SE Netherlands: evidence for 200 m of late Neogene and Quaternary surface uplift, in: D. Maddy, M.G. Macklin, J.C. Woodward (Eds.), River Basin Sediment Systems: Archives of Environmental Change, A.A. Balkema Publishers, Lisse, 2001, 503 pp.
[29] B. Hallet, L. Hunter, J. Bogen, Rates of erosion and sediment evacuation by glaciers: a review of field data and their implications, Glob. Planet. Change 12 (1996) 213–235.
[30] A. de Goër, P. Boivin, G. Camus, A. Gourgaud, G. Kieffer, J. Mergoil, P.-M. Vincent, Volcanologie de la Chaîne des Puys, Parc Naturel Régional des Volcans d'Auvergne, 1991, 126 pp.
[31] R. Braucher, D.L. Bourlès, E.T. Brown, F. Colin, J.-P.

Muller, J.-J. Braun, M. Delaune, A. Edou Minko, C. Lescouet, G.M. Raisbeck, F. Yiou, Application of in situ-produced cosmogenic ^{10}Be and ^{26}Al to the study of lateritic soil development in tropical forest: theory and examples from Cameroon and Gabon, Chem. Geol. 170 (2000) 95–111.

[32] J.W. Kirchner, R.C. Finkel, C.S. Riebe, D.E. Granger, J.L. Clayton, J.G. King, W.F. Megahan, Mountain erosion over 10 y, 10 k.y., and 10 m.y. time scales, Geology 29 (2001) 591–594.

[33] B. Heisinger, M. Niedermayer, F.J. Hartmann, G. Korschinek, E. Nolte, G. Morteani, S. Neumaier, C. Petitjean, P.W. Kubik, A. Synal, S. Ivy-Ochs, In-situ production of radionuclides at great depths, Nucl. Instrum. Methods Phys. Res. B 123 (1997) 341–346.

[34] B.P. Heisinger, Myonen-induzierte Produktion von Radionukliden, PhD Thesis, Technische Universität München, 1998.

[35] P.W. Kubik, S. Ivy-Ochs, J. Masarik, M. Frank, C. Schlüchter, ^{10}Be and ^{26}Al production rates deduced from an instantaneous event within the dendro-calibration curve, the landslide of Köfels, Oetz Valley, Austria, Earth Planet. Sci. Lett. 161 (1998) 231–241.

[36] D. Lal, In situ produced cosmogenic isotopes in terrestrial rocks, Annu. Rev. Earth Planet. Sci. 16 (1988) 355–388.

[37] O.C. Allkofer, Introduction to Cosmic Rays, Verlag Karl Thiemig, München, 1975.

[38] D. Lal, Cosmic ray labeling of erosion surfaces: in situ nuclide production rates and erosion models, Earth Planet. Sci. Lett. 104 (1991) 424–439.

[39] J.P. Larue, Les nappes alluviales de la Loire et de ses affluents dans le Massif Central et dans le Sud de bassin Parisien, étude géomorphologique, Clermont II, 1979.

[40] J.F. Pastre, Altération et paleoaltération des minéraux lourds des alluvions Pliocènes et Pleistocènes du bassin de l'Allier (Massif Central, France), Assoc. Rf. Etud. Quat. Bull. 3/4 (1986) 257–269.

[41] L.A. Tebbens, A. Veldkamp, W. Westerhoff, S.B. Kroonenberg, Fluvial incision and channel downcutting as a response to Late glacial and early Holocene climate change: the lower reach of the River Meuse (Maas), J. Quat. Sci. 14 (1999) 59–75.